

Nuclear medium effects from hadronic atoms

E. Friedman, A. Gal

Racah Institute of Physics, The Hebrew University, Jerusalem 91904, Israel

E-mail: elifried@vms.huji.ac.il, avragal@vms.huji.ac.il

Abstract. The state of the art in the study of π^- , K^- and Σ^- atoms, along with the in-medium nuclear interactions deduced for these hadrons, is reviewed. A special emphasis is placed on recent developments in \bar{K} -nuclear physics, where a strongly attractive density dependent K^- -nuclear potential of order 150–200 MeV in nuclear matter emerges by fitting K^- -atom data. This has interesting repercussions on \bar{K} quasibound *nuclear* states, on the composition of strange hadronic matter and on \bar{K} condensation in self bound hadronic systems.

1. Introduction

Hadronic atoms have played an important role in elucidating in-medium properties of hadron-nucleon (hN) interactions near threshold [1, 2]. Hadronic atom data consist primarily of strong interaction level shifts, widths and yields, derived from h^- -atom X-ray transitions. These data are analyzed in terms of optical potentials $V_{\text{opt}}^h = t_{hN}(\rho)\rho$ which are functionals of the nuclear density $\rho(r)$, capable of handling large data sets across the periodic table in order to identify characteristic entities that may provide a link between experiment and microscopic approaches. Here, $t_{hN}(\rho)$ is a density dependent in-medium hN t matrix at threshold, satisfying the low-density limit $t_{hN}(\rho) \rightarrow t_{hN}^{\text{free}}$, with the free-space t matrix t_{hN}^{free} , as $\rho \rightarrow 0$. A schematic summary of lessons gained by analyzing the available hadronic atom data in terms of optical potentials is given in Table 1, where the number of data points included in these analyses is shown in parentheses in the last column. A more exhaustive discussion of π^- , Σ^- and K^- atoms follows below.

Table 1. Hadronic atom scenarios which except for \bar{p} atoms are discussed in the present review.

hadron	Re V_{opt}	Im V_{opt}	comments
π^-	repulsive in bulk attractive on surface	moderate	excellent data (100) well understood
Σ^-	repulsive in bulk attractive outside	moderate	limited data (23) poorly understood
K^-	attractive <i>deep or shallow?</i>	absorptive	good data (65) <i>open problems</i>
\bar{p}	model dependent	very absorptive	excellent data (90)

2. Partial restoration of chiral symmetry from pionic atoms

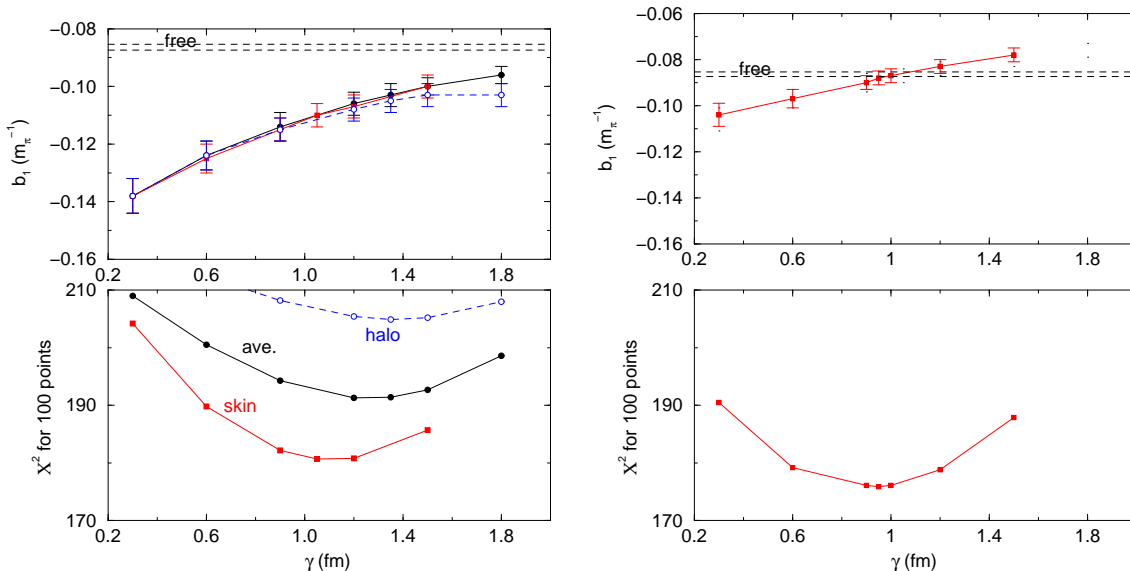


Figure 1. Fits to 100 π^- -atom data points from Ne to U as a function of γ . Left: density-independent (DI) b_1 . Right: density-dependent (DD) b_1 . Figure adapted from Ref. [2].

Density independent optical potential global fits to pionic atom data across the periodic table reveal an anomalous s -wave repulsion [1, 2], a major component of which is due to a too repulsive isovector πN amplitude b_1 with respect to the free-space value b_1^{free} . This is demonstrated on the l.h.s. of Fig. 1 which shows results of global fits to pionic atom data as a function of a parameter γ , related to the difference between neutron and proton rms radii:

$$r_n - r_p = \gamma \frac{N - Z}{A} + \delta. \quad (1)$$

Applying a finite-range folding with rms radius 0.9 fm to the p -wave part of V_{opt}^π , the resulting χ^2 minimum for a ‘skin’ neutron distribution is obtained at $\gamma = 1.1 \pm 0.1$ fm.¹ The r.h.s. of the figure shows results of global fits with empirical energy dependence imposed on the s -wave amplitudes b_0 and b_1 [4], and more importantly with a DD renormalization of b_1 :

$$b_1(\rho) = \frac{b_1}{1 - \frac{\sigma\rho}{m_\pi^2 f_\pi^2}}, \quad (2)$$

where $f_\pi = 92.4$ MeV is the pion weak decay constant and $\sigma \approx 50$ MeV is the πN σ term. Eq. (2) was derived by Weise [5] considering an in-medium extension of the Tomozawa-Weinberg (TW) LO chiral limit for b_1 in terms of f_π [6] which is then related to the quark condensate $\langle \bar{q}q \rangle$:

$$b_1(\rho) = -\frac{\mu_{\pi N}}{8\pi f_\pi^2(\rho)}, \quad \frac{f_\pi^2(\rho)}{f_\pi^2} = \frac{\langle \bar{q}q \rangle_\rho}{\langle \bar{q}q \rangle_0} \simeq 1 - \frac{\sigma\rho}{m_\pi^2 f_\pi^2}. \quad (3)$$

The figure makes it evident that the magnitude of b_1 on the r.h.s., following the DD renormalization, is systematically smaller than that on the l.h.s., and at the χ^2 minimum it agrees perfectly with b_1^{free} .

¹ For a recent discussion of the role of neutron distributions in hadronic atoms, see Ref. [3].

Table 2. Values of b_1 derived from density-independent fits to pionic atom data sets listed in Ref. [9]. For comparison, $b_1^{\text{free}} = -0.0864 \pm 0.0010 m_\pi^{-1}$ [10]. ‘Deep’ refers to $1s \pi^-$ ‘deeply bound’ states in ^{205}Pb [11] and $^{115,119,123}\text{Sn}$ [8] observed in $(d, ^3\text{He})$ experiments at GSI.

data	global ^{20}Ne to ^{238}U	light $N = Z$ + ‘deep’ $1s$ only	‘deep’ $1s$ only
points	100	20	8
$b_1(m_\pi^{-1})$	-0.104 ± 0.006	-0.104 ± 0.013	-0.130 ± 0.036

A similar conclusion was reached in Refs. [7, 8] from measurements of $1s$ ‘deeply bound’ pionic atoms of Sn isotopes. The advantage of using $1s$ ‘deeply bound’ levels is that the p -wave πN interaction plays there a secondary role, but this merit is more than compensated by the considerably increased errors associated with smaller data sets, as shown in Table 2. The uncertainty listed in the fourth column makes it clear that the ‘deeply bound’ atoms alone do not give conclusive evidence for the need to renormalize b_1 . In fact, Suzuki *et al.* [8] considered ‘deeply bound’ $1s$ levels in three Sn isotopes together with ‘normal’ $1s$ levels in ^{16}O , ^{20}Ne and ^{28}Si , 12 data points in total yielding $b_1 = -0.1149 \pm 0.0074 m_\pi^{-1}$. However, this small uncertainty excludes the uncertainty from the p -wave πN potential which was held fixed in their analysis. A more realistic uncertainty for this type of deduction is given in column 3 of the table.

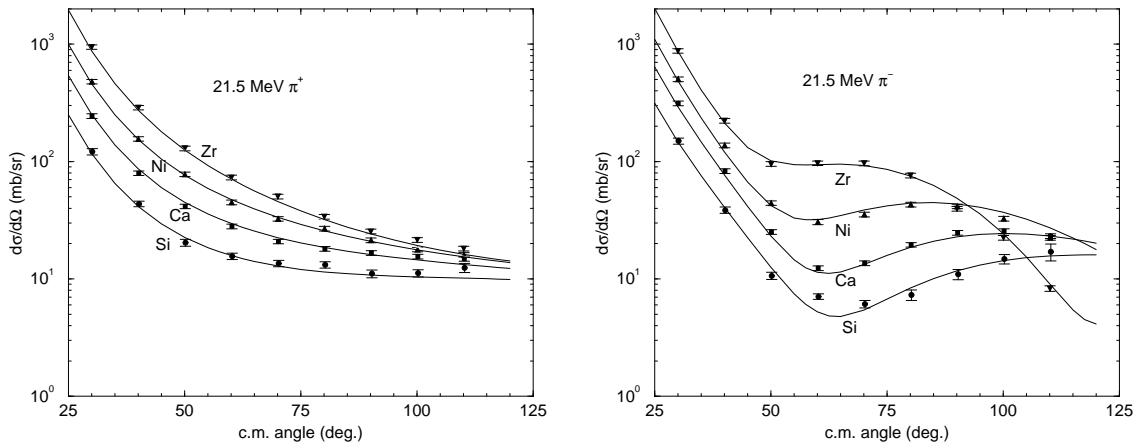


Figure 2. Low energy π^\pm nucleus elastic scattering angular distributions [12] reproduced with $b_1(\rho)$ ansatz, Eq. (2).

The renormalization of b_1 derived from pionic atoms is consistent with that shown recently to be also required in low energy π -nucleus scattering, as demonstrated in Fig. 2 for 21.5 MeV π^\pm scattered off isotopes of Si, Ca, Ni and Zr at PSI [12].

3. Σ Nuclear repulsion from Σ^- atoms

A vast body of (K^-, π^\pm) spectra indicate a repulsive and moderately absorptive Σ nuclear potential V^Σ , with a substantial isospin dependence [13, 14]. These data, including recent (π^-, K^+) spectra [15] and related DWIA analyses [16], provide credible evidence that Σ hyperons generally do not bind in nuclei. A repulsive component of a DD Σ nuclear potential was already

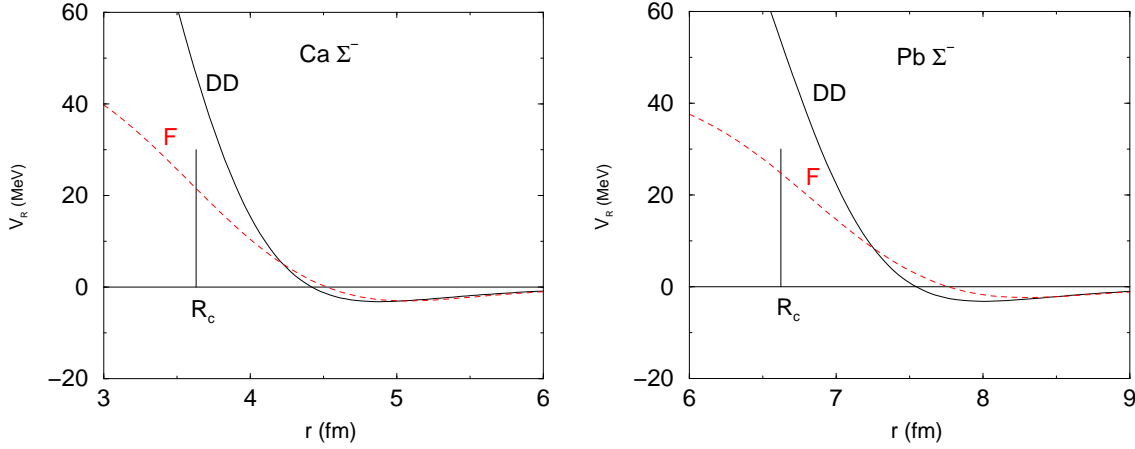


Figure 3. V_R^Σ from fits to Σ^- atoms [2]. The transition from attraction to repulsion occurs well outside of R_c , the half-density radius of the charge distribution in Ca (l.h.s.) and Pb (r.h.s.).

deduced in the mid 1990s from Σ^- atom data [17, 18], as shown in Fig. 3. In fact, V_R^Σ is attractive at low densities outside the nucleus, as enforced by the observed ‘attractive’ Σ^- atomic level shifts, changing into repulsion on approach of the nuclear radius. The precise magnitude and shape of V_R^Σ within the nucleus, however, are model dependent as demonstrated by the difference between potentials DD and F (defined in the Appendix). This repulsion bears interesting consequences for the balance of strangeness in the inner crust of neutron stars, primarily by delaying to higher densities, or even aborting the appearance of Σ^- hyperons, as shown in Fig. 4.

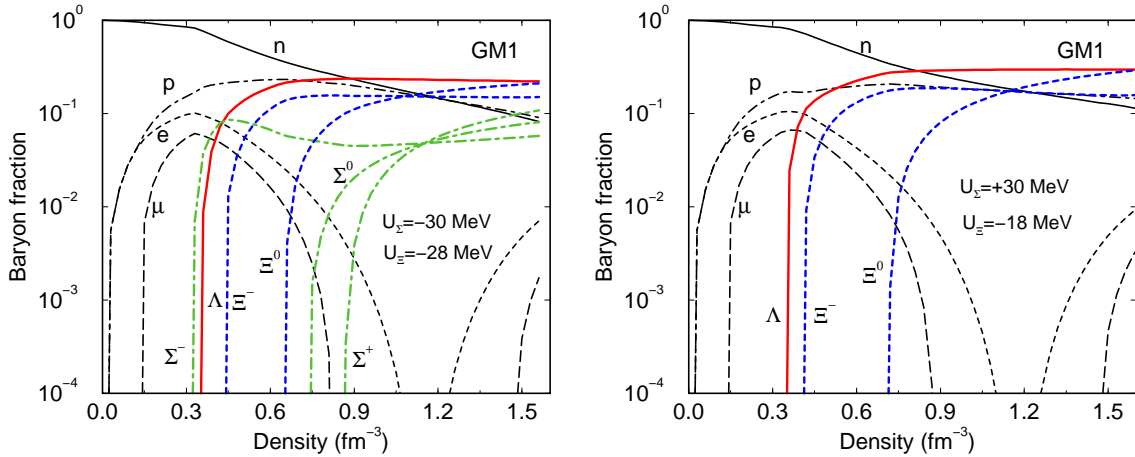


Figure 4. RMF calculations of baryon & lepton fractions in neutron star matter for different scenarios of hyperon nuclear potential depths U_Y . Figure adapted from Ref. [19].

The G -matrices constructed from Nijmegen soft-core potential models have progressed throughout the years to produce Σ repulsion in symmetric nuclear matter, as demonstrated in Table 3 using the parametrization

$$V_R^\Sigma = V_0^\Sigma + \frac{1}{A} V_1^\Sigma \mathbf{T}_A \cdot \mathbf{t}_\Sigma . \quad (4)$$

Table 3. Isoscalar and isovector Σ nucleus potentials, Eq. (4) in MeV, calculated in Nijmegen soft-core potential models [20] at $k_F = 1.35 \text{ fm}^{-1}$, corresponding to nuclear-matter density.

	97f	04d	06d	08a	08b	phenom.	Ref.
V_0^Σ	-13.9	-26.0	-1.2	+13.4	+20.3	$+30 \pm 20$	[2, 16]
V_1^Σ	-30.4	+30.4	+52.6	+64.5	+85.2	$\approx +80$	[21]

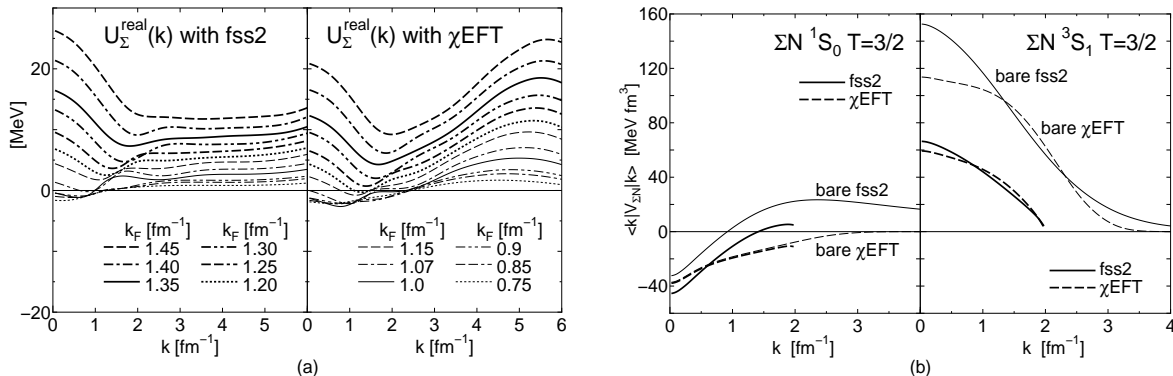


Figure 5. Left: Isoscalar Σ nuclear potentials calculated in two models, Refs. [22, 23]. Right: $(\Sigma N)_{T=3/2}$ potentials calculated in these models. Figure adapted from Ref. [24].

In the latest Nijmegen ESC08 model [20], this repulsion is dominated by repulsion in the $T = 3/2$, ${}^3S_1 - {}^3D_1$ ΣN channel where a strong short distance Pauli exclusion repulsion for quarks arises in SU(6) quark-model RGM [22] and in chiral EFT [23] calculations, as seen on the r.h.s. of Fig. 5. These model calculations also lead to Σ nuclear repulsion, shown in momentum space on the l.h.s. of the figure. A strong repulsion appears also in a recent SU(3) chiral perturbation calculation [25] which yields $V_0^\Sigma \approx 60 \text{ MeV}$. Phenomenologically $V_0^\Sigma > 0$ and $V_1^\Sigma > 0$, as listed in the table, and the resulting Σ -nuclear potential V_R^Σ is repulsive.²

4. \bar{K} -nucleus potentials from K^- atoms

The gross features of low-energy $\bar{K}N$ physics are encapsulated in the leading-order Tomozawa-Weinberg (TW) vector term of the chiral effective Lagrangian [6]. The Born approximation for the \bar{K} -nuclear potential $V_{\text{TW}}^{\bar{K}}$ due to this TW interaction term yields a sizable attraction:

$$V_{\text{TW}}^{\bar{K}} = -\frac{3}{8f_\pi^2} \rho \sim -55 \frac{\rho}{\rho_0} \quad (\text{MeV}) \quad (5)$$

for $\rho_0 = 0.16 \text{ fm}^{-3}$. Iterating the TW term plus the less significant NLO terms, within an *in-medium* coupled-channel approach constrained by the $\bar{K}N - \pi\Sigma - \pi\Lambda$ data near the $\bar{K}N$ threshold, roughly doubles this \bar{K} -nucleus attraction [29]. A major uncertainty in these chirally based studies arises from fitting the $\Lambda(1405)$ resonance by the imaginary part of the $(\pi\Sigma)_{I=0}$

² In the case of ${}^4_2\text{He}$, the only known quasibound Σ hypernucleus [26, 27], the isovector term provides substantial attraction owing to the small value of A towards binding the $T = 1/2$ hypernuclear configuration, while the isoscalar repulsion reduces the quasibound level width [28].

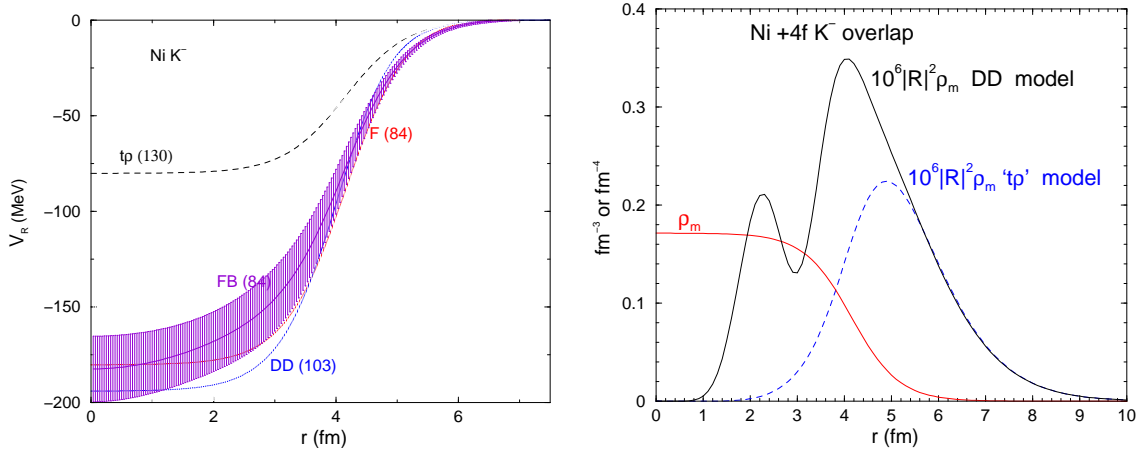


Figure 6. Left: $V_R^{\bar{K}}$ in Ni from global fits to 65 K^- atom data points, with χ^2 values in parentheses [2]. The shaded area approximates the uncertainty in the Fourier-Bessel fit. Right: Overlap of K^- atomic $4f$ radial wavefunctions R squared with Ni matter density ρ_m .

amplitude calculated within the same coupled channel chiral scheme. Yet, irrespective of this uncertainty, the $\Lambda(1405)$ which may be viewed as a K^-p quasibound state quickly dissolves in the nuclear medium at low density, so that the repulsive free-space scattering length a_{K^-p} , as function of ρ , becomes *attractive* well below ρ_0 . Adding the weakly density dependent $I = 1$ attractive scattering length a_{K^-n} , the resulting in-medium $\bar{K}N$ isoscalar scattering length $b_0(\rho) = \frac{1}{2}(a_{K^-p}(\rho) + a_{K^-n}(\rho))$ translates into a strongly attractive $V^{\bar{K}}$ [30, 31]:

$$V_R^{\bar{K}}(\rho) \sim -\frac{2\pi}{\mu_{KN}} \text{Re } b_0(\rho_0) \rho_0 \frac{\rho}{\rho_0} \approx -110 \frac{\rho}{\rho_0} \quad (\text{MeV}). \quad (6)$$

Shallower potentials, $V_R^{\bar{K}}(\rho_0) \sim -(40 - 60)$ MeV, were obtained by imposing a Watson-like self-consistency requirement [30, 32]. It turns out, however, that stronger attraction, $V_R^{\bar{K}}(\rho_0) \sim -(80 - 90)$ MeV, arises in similar chiral approaches [33] when imposing the same requirement while considering the energy dependence of the in-medium $\bar{K}N$ scattering amplitude below threshold [34].

Comprehensive fits to the strong-interaction shifts and widths of K^- -atom levels, begun in the mid 1990s [35], have yielded DD deeply attractive and strongly absorptive optical potentials with nuclear-matter depth $-V_R^{\bar{K}}(\rho_0) \sim (150 - 200)$ MeV at threshold [35]. The l.h.s. of Fig. 6 illustrates for ^{58}Ni the real part of \bar{K} -nucleus potentials obtained from a global fit to the data in several models and, in parentheses, the corresponding values of χ^2 for 65 K^- -atom data points. A model-independent Fourier-Bessel (FB) fit [36] is also shown, within an error band. Just three terms in the FB series, added to a $t\rho$ potential, suffice to achieve a χ^2 as low as 84 and to make the potential extremely deep, in agreement with the density-dependent best-fit potentials DD and F. In particular, potential F provides by far the best fit ever reported for any global K^- -atom data fit [37], and the lowest χ^2 value as reached by the FB method.

Shown on the r.h.s. of Fig. 6 are overlaps of the $4f$ atomic radial wavefunction squared with the matter density ρ_m in ^{58}Ni for two of the models exhibited on the l.h.s. of the figure. The $4f$ atomic orbit is the last circular K^- atomic orbit from which the K^- meson undergoes nuclear absorption. The figure demonstrates that, whereas this overlap for the shallower $t\rho$ potential peaks at nuclear density of order 10% of ρ_0 , it peaks at about 60% of ρ_0 for the deeper DD potential and has a secondary peak well inside the nucleus. The double-peak structure indicates

Table 4. Full and reduced K^- atom data set fits. The reduced set consists of $2p, 3d, 4f, 5g, 7i$ shifts, widths and yields in C, Si, Ni, Sn and Pb targets, respectively [39].

N	shallow potential			deep potential		
	Re $b(\rho_0)$	Im $b(\rho_0)$	χ^2	Re $b(\rho_0)$	Im $b(\rho_0)$	χ^2
65	0.62±0.05	0.93±0.04	130	1.44±0.03	0.59±0.03	84
15	0.78±0.13	0.92±0.11	44	1.47±0.05	0.55±0.06	26

the existence of a K^- strong-interaction $\ell = 3$ quasibound state for the DD potential. It is clear that whereas within the $t\rho$ potential there is no sensitivity to the interior of the nucleus, the opposite holds for the density dependent F potential which accesses regions of full nuclear density. This owes partly to the smaller imaginary part of F.

Given the repercussions of deeply attractive potentials on the equation of state of dense matter, it is important to explore the stability of these best-fit solutions to variations in the data selection and the fitting procedure. The most obvious question to ask is whether the resulting best-fit potentials depend strongly on the size, composition and accuracy of the data set studied. Regarding size and composition, following an earlier discussion [38] it has been observed recently [39] that the DD deep potentials and the DI relatively shallow potentials, as well as the superiority of DD to DI in terms of quality of fit, persist upon decreasing the size of the data set. This is demonstrated in Table 4 upon reducing the 65 data point global set down to 15 data points from five targets spread over the entire periodic table (C, Si, Ni, Sn, Pb). Similar results hold for any four out of these five targets. It makes sense then to repeat some of the 30 – 40 years old K^- atom measurements, making use of modern techniques, in order to acquire a minimum size canonical set of data with reduced statistical errors and with common systematics. For the specific set proposed in Ref. [39], the (lower level) widths are directly measurable yet not excessively large to make it difficult to observe the feeding X-ray transition above the background. Similarly, the relative yields of the upper to lower level transitions are of the order of 10% and higher. Fitting to such a data set with improved accuracy could resolve the issue of deep vs. shallow potentials and determine how deep is ‘deep’.

A fairly new and independent evidence in favor of extremely deep \bar{K} -nucleus potentials is provided by (K^-, n) and (K^-, p) spectra taken at KEK on ^{12}C [40] and very recently also on ^{16}O [41] at $p_{K^-} = 1$ GeV/c. The ^{12}C spectra are shown on the l.h.s. of Fig. 7, where the solid lines represent calculations (outlined in Ref. [43]) using potential depths in the range 160 – 190 MeV. The dashed lines correspond to using relatively shallow potentials of depth about 60 MeV which may be considered excluded by these data. However, Magas *et al.* [44] have recently expressed concerns about protons of reactions other than those *directly* emanating in the (K^-, p) reaction and which could explain part of the bound-state region of the measured spectrum without invoking a very deep \bar{K} -nuclear potential. A sufficiently deep potential would allow quasibound states bound by over 100 MeV, for which the major $\bar{K}N \rightarrow \pi\Sigma$ decay channel is blocked, resulting in relatively narrow \bar{K} -nuclear states. Of course, a fairly sizable extrapolation is involved in this case using an energy-independent potential determined largely near threshold. Furthermore, the best-fit V_I^K imaginary depths of 40–50 MeV imply that \bar{K} -nuclear quasibound states are broad, as studied in Refs. [37, 47].

A robust consequence of the sizable \bar{K} -nucleus attraction is that K^- condensation, when hyperon degrees of freedom are ignored, could occur in neutron star matter at about 3 times nuclear matter density, as shown on the r.h.s. of Fig. 7. Comparing it with Fig. 4 for neutron stars, but where strangeness materialized through hyperons, one may ask whether \bar{K} mesons

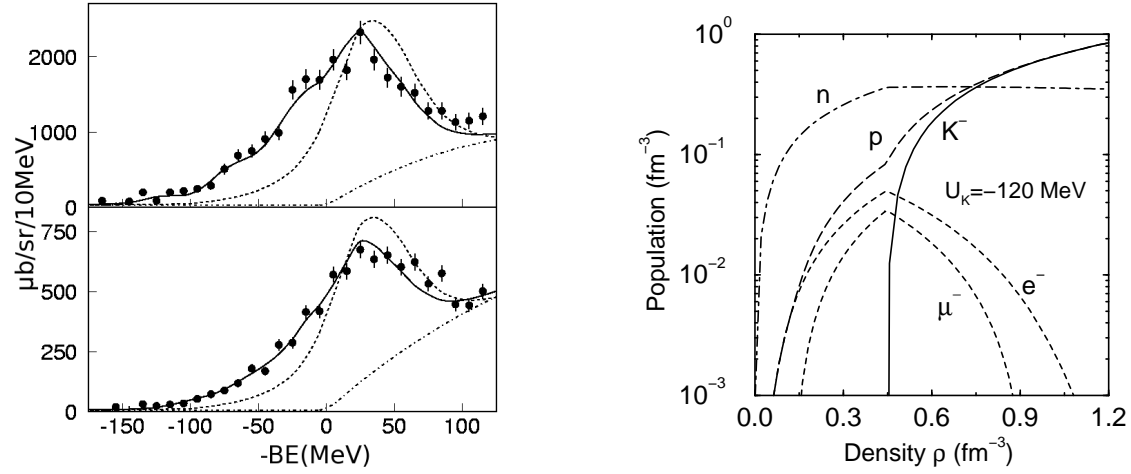


Figure 7. Left: KEK-PS E548 missing mass (K^- , n) (upper) & (K^- , p) (lower) spectra on ^{12}C at $p_{K^-} = 1 \text{ GeV}/c$ [40]. Right: calculated neutron-star population as a function of density. The neutron density stays nearly constant once kaons condense [42].

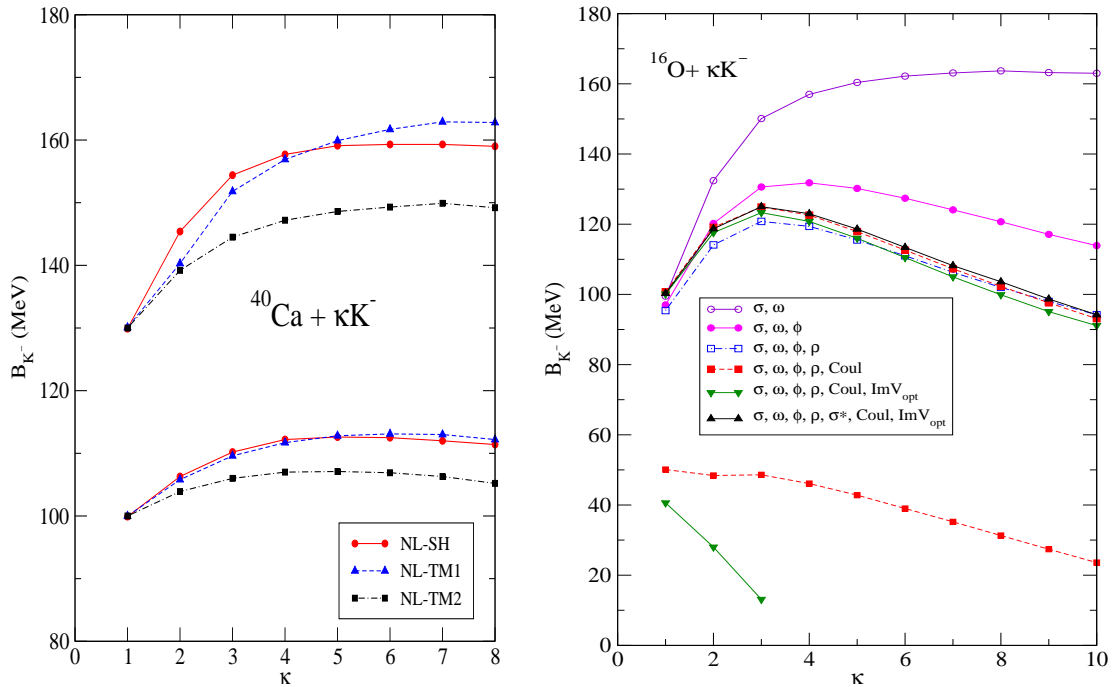


Figure 8. Saturation of K^- separation energy B_{K^-} in RMF calculations of multi K^- nuclei as a function of the number κ of K^- mesons [48]. Left: RMF model dependence. Right: dependence on RMF ingredients.

condense also in the presence of hyperons. This question was posed within RMF calculations of neutron star matter long ago and answered negatively [45, 46], but only recently it was posed

for strange hadronic matter in Ref. [48] by calculating multi- \bar{K} nuclear configurations. Fig. 8 demonstrates a remarkable saturation of K^- separation energies B_{K^-} calculated in multi- K^- nuclei, independently of the applied RMF model as shown on the l.h.s. for three different nuclear RMF schemes. The r.h.s. of the figure demonstrates that this saturation persists already in the most straightforward $\sigma + \omega$ model, primarily owing to the repulsion induced by the vector ω field between like \bar{K} mesons. The additional vector fields ρ and ϕ only add repulsion, thus strengthening the saturation. The effect of $V_I^{\bar{K}}$ is noticeable only below $B_{\bar{K}} \approx 100$ MeV, as seen by the departure of the lowest green line with respect to the lowest red line.

The saturation values of B_{K^-} do not allow conversion of hyperons to \bar{K} mesons through the strong decays $\Lambda \rightarrow p + K^-$ or $\Xi^- \rightarrow \Lambda + K^-$ in multi-strange hypernuclei, which therefore remain the lowest-energy configuration for multi-strange systems [49]. This provides a powerful argument against \bar{K} condensation in the laboratory, under strong-interaction equilibrium conditions [48]. It does not apply to kaon condensation in neutron stars, where equilibrium configurations are determined by weak-interaction conditions. This work has been recently generalized to multi- K^- hypernuclei [50].

Appendix: density dependent optical potentials

Here we specify the functional form of two density dependent optical potentials used in studies of hadronic atoms. For a recent application to K^- atoms, see Table 1 of Ref. [37].

- The DD form is based on modifying the effective scattering length b_0 (e.g. Eq. (6)):

$$V^h(r) \sim -\frac{2\pi}{\mu_{hN}} b_0 \rho(r) \Rightarrow b_0 \rightarrow b_0 + B_0 \left\{ \frac{\rho(r)}{\rho_0} \right\}^\alpha, \quad \alpha > 0, \quad (\text{A.1})$$

where $\rho_0 = 0.16 \text{ fm}^{-3}$ is a central nuclear density. It is possible then to respect the ‘low density limit’ by keeping b_0 fixed, $b_0 = b_0^{\text{free}}$, while varying the parameters B_0 and α .

- The F form is based on modifying b_0 as follows:

$$b_0 \rightarrow B_0 F(r) + b_0 [1 - F(r)]. \quad (\text{A.2})$$

The density-like function $F(r)$ is defined as

$$F(r) = \frac{1}{e^x + 1}, \quad x = \frac{r - R_x}{a_x}. \quad (\text{A.3})$$

Clearly, $F(r) \rightarrow 1$ for $r \ll R_x$ which defines an internal region and similarly $[1 - F(r)] \rightarrow 1$ for $r \gg R_x$ which defines an external region. Thus R_x forms an approximate border between internal and external regions, and if R_x is close to the nuclear surface then the two regions do correspond to the high-density and low-density regions of nuclei, respectively. In global fits across the periodic table, R_x is parametrized as $R_x = R_{x0} A^{1/3} + \delta_x$ and the parameters B_0 , R_{x0} and δ_x are varied upon in the least-squares fit, while gridding on values of a_x around 0.5 fm. The parameter b_0 may be held fixed at its free hN value, but the results often depend very little on its precise value.

Acknowledgments

On the occasion of Gerry Brown’s 85th birthday Festschrift, we dedicate this mini review to him who commissioned our two past reviews [1, 2] on similar subjects. This work was supported in part by the SPHERE collaboration within the HadronPhysics2 Project No. 227431 of the EU initiative FP7.

References

- [1] Batty C J, Friedman E and Gal A 1997 *Phys. Rept.* **287** 385
- [2] Friedman E and Gal A 2007 *Phys. Rept.* **452** 89, and references therein
- [3] Friedman E 2009 *Hyp. Int.* **193** 33, and references therein
- [4] Friedman E and Gal A 2004 *Phys. Lett. B* **578** 85
- [5] Weise W 2001 *Nucl. Phys. A* **690** 98c
- [6] Tomozawa Y 1966 *Nuovo Cimento A* **46** 707, Weinberg S 1966 *Phys. Rev. Lett.* **17** 616
- [7] Kolomeitsev E E, Kaiser N and Weise W 2003 *Phys. Rev. Lett.* **90** 092501
- [8] Suzuki K *et al.* 2004 *Phys. Rev. Lett.* **92** 072302
- [9] Friedman E and Gal A 2003 *Nucl. Phys. A* **724** 143
- [10] Marton J 2007 *Nucl. Phys. A* **790** 328c
- [11] Geissel H *et al.* 2002 *Phys. Rev. Lett.* **88** 122301
- [12] Friedman E *et al.* 2004 *Phys. Rev. Lett.* **93** 122302, 2005 *Phys. Rev. C* **72** 034609
- [13] Dover C B, Millener D J and Gal A 1989 *Phys. Rept.* **184** 1, and references therein
- [14] Bart S *et al.* [BNL E887] 1999 *Phys. Rev. Lett.* **83** 5238
- [15] Noumi H *et al.* [KEK E438] 2002 *Phys. Rev. Lett.* **89** 072301, 2003 *Phys. Rev. Lett.* **90** 049902(E), Saha P K *et al.* 2004 *Phys. Rev. C* **70** 044613
- [16] Kohno M, Fujiwara Y, Watanabe Y, Ogata K and Kawai M 2004 *Prog. Theor. Phys.* **112** 895, 2006 *Phys. Rev. C* **74** 064613, Harada T and Hirabayashi Y 2005 *Nucl. Phys. A* **759** 143, 2006 **767** 206
- [17] Batty C J, Friedman E and Gal A 1994 *Phys. Lett. B* **335** 273, *Prog. Theor. Phys. Suppl.* **117** 227
- [18] Mareš J, Friedman E, Gal A and Jennings B K 1995 *Nucl. Phys. A* **594** 311
- [19] Schaffner-Bielich J 2010 *Nucl. Phys. A* **835** 279, and references therein
- [20] Rijken Th A, Nagels M M and Yamamoto Y 2010 *Nucl. Phys. A* **835** 160, and references therein
- [21] Dover C B, Gal A and Millener D J 1984 *Phys. Lett. B* **138** 337
- [22] Fujiwara Y, Suzuki Y and Nakamoto C 2007 *Prog. Part. Nucl. Phys.* **58** 439, and references therein
- [23] Polinder H, Haidenbauer J and Meißner U G 2006 *Nucl. Phys. A* **779** 244
- [24] Kohno M 2010 *Phys. Rev. C* **81** 014003
- [25] Kaiser N 2005 *Phys. Rev. C* **71** 068201
- [26] Hayano R S *et al.* 1989 *Phys. Lett. B* **231** 355
- [27] Nagae T *et al.* [BNL E905] 1998 *Phys. Rev. Lett.* **80** 1605
- [28] Harada T 1998 *Phys. Rev. Lett.* **81** 5287
- [29] Borasoy B, Nißler R and Weise W 2005 *Eur. Phys. J. A* **25** 79
- [30] Cieplý A, Friedman E, Gal A and Mareš J 2001 *Nucl. Phys. A* **696** 173
- [31] Weise W and Härtle R 2008 *Nucl. Phys. A* **804** 173
- [32] Ramos A and Oset E 2000 *Nucl. Phys. A* **671** 481
- [33] Cieplý A and Smejkal J 2010 *Eur. Phys. J. A* **43** 191
- [34] Cieplý A, Friedman E, Gal A, Gazda D and Mareš J 2011 *Phys. Lett. B* **702** 402, see also Cieplý A, Friedman E, Gal A and Krejčířík V 2011 *Phys. Lett. B* **698** 226
- [35] Friedman E, Gal A and Batty C J 1993 *Phys. Lett. B* **308** 6, 1994 *Nucl. Phys. A* **579** 518
- [36] Barnea N and Friedman E 2007 *Phys. Rev. C* **75** 022202(R)
- [37] Mareš J, Friedman E and Gal A 2006 *Nucl. Phys. A* **770** 84
- [38] Friedman E, Gal A, Mareš J and Cieplý A 1999 *Phys. Rev. C* **60** 024314
- [39] Friedman E 2011 *Int. J. Mod. Phys. A* **26** 468 (Proc. Int. Conf. on Meson Physics, Krakow 2010)
- [40] Kishimoto T 2007 *et al.* [KEK E548] *Prog. Theor. Phys.* **118** 181
- [41] Kishimoto T 2009 *Nucl. Phys. A* **827** 321c
- [42] Glendenning N K and Schaffner-Bielich J 1999 *Phys. Rev. C* **60** 025803
- [43] Yamagata J, Nagahiro H and Hirenzaki S 2006 *Phys. Rev. C* **74** 014604
- [44] Magas V K, Yamagata-Sekihara J, Hirenzaki S, Oset E and Ramos A 2010 *Phys. Rev. C* **81** 024609
- [45] Knorren R, Prakash M and Ellis P J 1995 *Phys. Rev. C* **52** 3470
- [46] Schaffner J and Mishustin I N 1996 *Phys. Rev. C* **53** 1416
- [47] Gazda D, Friedman E, Gal A and Mareš J 2007 *Phys. Rev. C* **76** 055204
- [48] Gazda D, Friedman E, Gal A and Mareš J 2008 *Phys. Rev. C* **77** 045206
- [49] Schaffner-Bielich J and Gal A 2000 *Phys. Rev. C* **62** 034311, and references therein
- [50] Gazda D, Friedman E, Gal A and Mareš J 2009 *Phys. Rev. C* **80** 035205